

# Formation mechanism of hexagonal structure of basalt columnar joints based on Mechanics of Materials and infinitesimal method

Zirong Wang<sup>1</sup>, Siyun Zhou<sup>2</sup>

<sup>1</sup>School of Reliability and System Engineering, Beihang University, Beijing, China

<sup>2</sup>School of Physics, Beihang University, Beijing, China

**Abstract:** The perfect hexagon showed by columnar jointed basalt gets great public appeal. However, the accurate illustration was not given. A new explanation, which has rigid calculation, is proposed here for their origin. With the cooling of basalt, the distribution of stress changes while the normal stress equal to the tensile strength of basalt. Using an equation as  $\tau_\theta = \tau_f$ , where  $\tau_\theta$  is the force tangentially acting on the unit shear boundaries and  $\tau_f$  represents the shear strength of basalt, to indicate the condition of the shear fracture. The result of numerical calculation shows that cleavages appear at angles of  $\pm 59.53^\circ$  with the  $\sigma_1$ , which effectively illustrate why the columnar jointed occur in conjugate pairs with  $\sim 120^\circ$  angle between cleavages. The angle depends on the internal friction angle, the cohesive force, the tensile strength and Poisson's ratio of basalt. Other factors on the sides and diameter of columnar jointed, such as the velocity of cooling and components of magma, will be deeply researched in our future work.

**Keywords:** columnar jointed basalt, the internal friction angle, the cohesive force, the tensile strength, Poisson's ratio, the percentage composition of quartz

## 1. Introduction

Basalt formed after the eruption and cooling of magma, and the rocks often broke down during cooling. It is observed in fields that the broken basalt is usually hexagonal, and a few are pentagonal, quadrilateral and triangular.

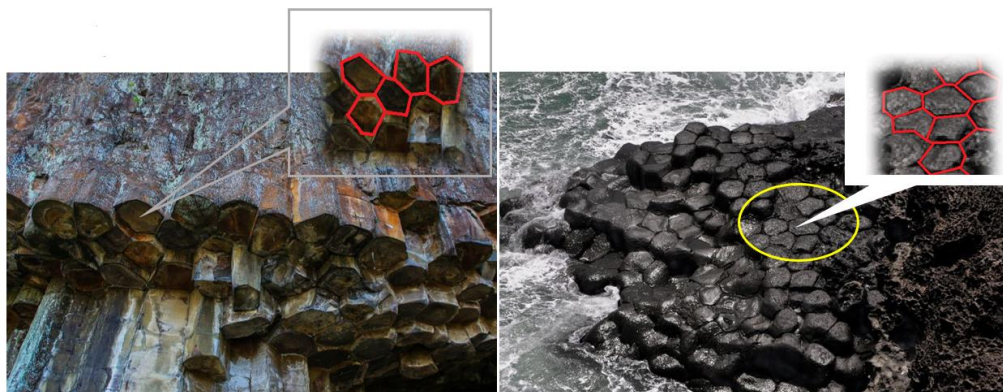


Figure 1: The photos of basalt columnar joints

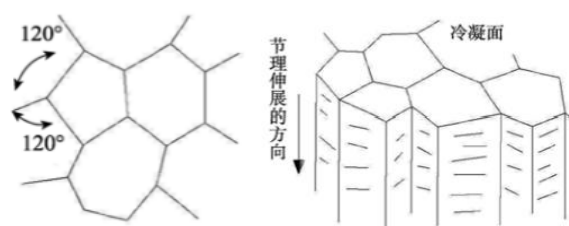


Figure 2: Simplified schematic diagram of basalt columnar joints

According to statistics, the phenomenon of basalt columnar joints being hexagonal and the inner angle being  $120^\circ$  is widespread [1].

|   | No. columns | Avg no. sides | $\Sigma N$ | Mean column diameter (cm) | Mean side length <L> (cm) | $\sigma(L)$ | $\sigma(L)/\langle L \rangle$ | column top area <A> (cm <sup>2</sup> ) | $\sigma(A)$ | $\sigma(A)/\langle A \rangle$ | Mean internal angle $^\circ$ | $\sigma(\theta)$ | $\sigma(\theta)/\langle \theta \rangle$ |
|---|-------------|---------------|------------|---------------------------|---------------------------|-------------|-------------------------------|--|-------------|-------------------------------|------------------------------|------------------|---|
| Locality 1 (colonnade)                          | 71          | 5.7           | 0.80       | 77.5                      | 38.3                      | 18.2        | 0.476                         | 3157                                   | 1571        | 0.497                         | 117.8                        | 19.5             | 0.166                                   |
| Locality 2 (colonnade)                          | 138         | 5.8           | 0.86       | 83.4                      | 40.1                      | 17.4        | 0.434                         | 3709                                   | 1278        | 0.345                         | 118.2                        | 18               | 0.152                                   |
| Locality 3 (colonnade)                          | 53          | 5.9           | 0.93       | 91.8                      | 41.8                      | 18.3        | 0.439                         | 4329                                   | 2124        | 0.491                         | 118.9                        | 22.6             | 0.190                                   |
| Locality 5 (colonnade)                          | 68          | 5.9           | 0.87       | 113.5                     | 53.9                      | 24.6        | 0.456                         | 7520                                   | 4059        | 0.540                         | 118.7                        | 19.2             | 0.162                                   |
| Locality 6 (colonnade)                          | 100         | 6.1           | 0.87       | 74.6                      | 33                        | 16.7        | 0.506                         | 2836                                   | 1654        | 0.583                         | 120.7                        | 21.8             | 0.180                                   |
| Locality 8 (colonnade)                          | 37          | 6.0           | 0.79       | 87.8                      | 41.8                      | 18.3        | 0.439                         | 4326                                   | 1992        | 0.461                         | 119.7                        | 18.4             | 0.153                                   |
| Locality 4 (entablature)                        | 58          | 5.9           | 0.62       | 24.5                      | 11.6                      | 6.01        | 0.518                         | 308.5                                  | 202.7       | 0.657                         | 119.1                        | 19.3             | 0.162                                   |
| Locality 7 (entablature)                        | 172         | 5.3           | 1.20       | 21.4                      | 11.9                      | 5.04        | 0.424                         | 271.1                                  | 154.1       | 0.568                         | 111.9                        | 25.2             | 0.225                                   |
| Locality 10 (hyaloclastite)                     | 13          | 5.5           | 1.11       |                           | 16.4                      | 6.84        | 0.417                         |  |             |                               |                              |                  |   |
| Giant's Causeway [1]                            | 76          | 5.9           | 0.78       |                           | 27.7                      | 13.7        | 0.493                         |  |             | 0.338                         | 119                          | 13.7             | 0.126                                   |
| Giant's Causeway [2]                            | 400         | 5.7           | 0.80       |                           |                           |             |                               |  |             |                               |                              |                  |   |
| Devil's Postpile [3]                            | 400         | 5.5           | 0.92       |                           |                           |             |                               |  |             |                               |                              |                  |   |
| Mount Rodeix, Auvergne [3]                      | 200         | 5.2           | 1.06       |                           |                           |             |                               |  |             |                               |                              |                  |   |
| Aloe lava lake [4]                              | 26          | 4.8           | 1.62       |                           |                           |             |                               |  |             | 0.77                          |                              |                  |   |
| Aloe lava lake [4]                              | 72          | 4.6           | 1.72       |                           |                           |             |                               |  |             | 1.0                           |                              |                  |   |
| Makaopuhi lava lake [4]                         | 55          | 4.4           | 1.86       |                           |                           |             |                               |  |             | 0.833                         |                              |                  |   |
| Paycuqui ignimbrite, Cerro Galan, Argentina [5] |             | 4.5           | 1.72       | 75                        |                           |             |                               |  |             |                               |                              |                  |   |
| Poisson model [6]                               | 46000       | 6.0           | 1.33       |                           |                           |             |                               |  |             |                               |                              |                  |   |
| Anti-clustered (random close-packing) model [7] | 675         | 6.0           | 0.80       |                           |                           |             |                               |  |             |                               |                              |                  |   |
| Mature (regular close-packing) model [7]        | 500         | 6.0           | 0.54       |                           |                           |             |                               |  |             | 0.152                         |                              |                  |   |
| Numerical model, $t = 10$ [8]                   | 110         | 6.0           | 1.26       |                           |                           |             |                               |  |             | 0.464                         |                              |                  |   |
| Numerical model, $t = 20$ [8]                   | 99          | 6.0           | 1.03       |                           |                           |             |                               |  |             | 0.368                         |                              |                  |   |
| Numerical model, $t = 280$ [8]                  | 93          | 6.2           | 0.80       |                           |                           |             |                               |  |             | 0.283                         |                              |                  |   |
| Starch, $d = 7\text{ mm}$ [9]                   | 100         | 6.8           | 1.54       |                           |                           |             |                               |  |             | 0.357                         |                              |                  |   |
| Starch, $d = 11\text{ mm}$ [9]                  | 100         | 6.3           | 1.10       |                           |                           |             |                               |  |             | 0.429                         |                              |                  |   |
| Starch, $d = 19\text{ mm}$ [9]                  | 100         | 6.9           | 1.49       |                           |                           |             |                               |  |             | 0.497                         |                              |                  |   |

Figure 3: Statistics of inner angle and side length of columnar joints

After summarizing previous studies, there are two mainstream views:

1) Cooling makes the volume of the rock shrink, thus accounting for the breakdown of it and the show of columnar joints [2] [3].

2) In the process of magma cooling, the top layer of the rock formation is in a cooler atmosphere or in cooler water, but the bottom layer is at a higher temperature, thus there is an obvious temperature gradient between the top layer and the bottom layer. In the mean time, Rayleigh-Bénard convection occurs in a limited range of thickness below the solid-liquid boundary of the magma, forming a hexagonal "lattice" of convection (figure 2). In the process of cooling, the hexagonal lattice extends downward and finally forms columnar joints with the downward movement of the solid-liquid boundary [4] [5].

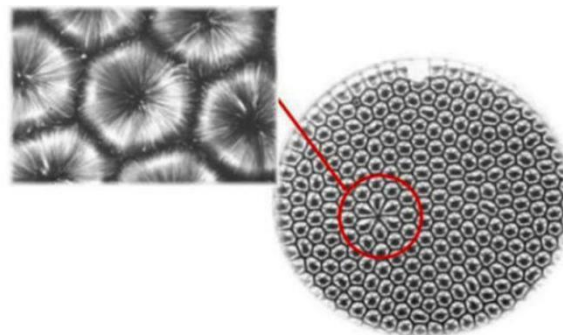


Figure 4: The vertical view of Rayleigh-Bénard convection

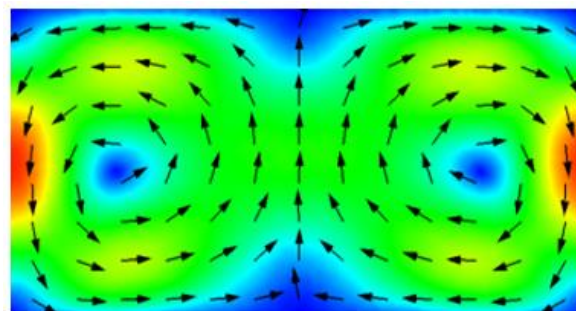


Figure 5: The side-view mimetic diagram of Rayleigh-Bénard convection

In this article analysis about the two opinions are as follows:

1) Viewpoint one holds that the rock fracture occurs under the action of tensile stress, but it is observed in the field that the fracture surface of basalt columnar joints is relatively flat, and some of the surfaces even appear scratches, which is inconsistent with the point.

2) Viewpoint 2 take the attitude that local Rayleigh-Bénard convection occurs during the cooling of the magma, so the flowing liquid will lead to the directional movement of the crystalline substance contained therein, showing the streamline of the Rayleigh-Bénard convection. However, this directional arrangement of crystalline substance in basalt columnar joints is not found in the field observations.

In summary, we consider that basalt has both tensile stress and shear stress in the process of cooling and rupture, and shear rupture takes place in basalt under the action of the two stresses, with columnar joints showing hexagonal.

## 2. Theoretical arithmetic

### 2.1 Model building

Using infinitesimal method to study basalt, we consider that basalt is isotropic, which means the force it bears is the same in all directions. However, because of the small local differences, the forces the infinitesimal bears in the two directions  $\sigma_1, \sigma_2$  are slightly different (on assumption that  $\sigma_1 > \sigma_2, \sigma_1 \approx \sigma_2$ ). So that little deformation occurs (Figure 6). At the same time, the tensile stress  $\sigma_1$  basalt bears is approximately equal to its tensile strength, and basalt is in the stage of imminent rupture.

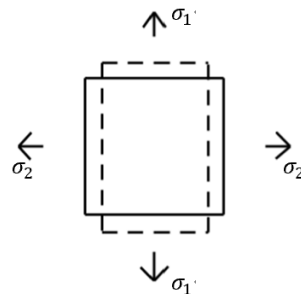


Figure 6: Schematic illustration of the stress deformation of the infinitesimal

Note 1: the solid line is in the stage before deformation and the dashed line is after deformation

The deformation trend of the infinitesimal will change the tensile stress  $\sigma_2$  and change the direction of the rock rupture. Let  $\sigma_3$  be the changed tensile stress, which is related to the Poisson's ratio of basalt. The Poisson's ratio of basalt is 0.23-0.32 [6], which is affected by temperature. When temperature increases, the toughness of basalt increases, and the Poisson ratio is smaller. When temperature decreases, the brittleness of rock increases, the Poisson ratio is larger. We use the average value in this paper, i.e.  $\nu = 2.8$ . Then the changed tensile stress  $\sigma_3$  is

$$\sigma_3 = \sigma_2 + \frac{\nu}{1 - \nu} \sigma_1 = \frac{1}{1 - \nu} \sigma_1 > \sigma_1$$

The force of the redistributed tensile stress on the infinitesimal is shown below

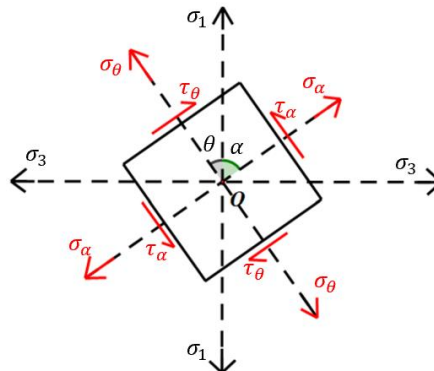


Figure 7: The stress on the infinitesimal

$\sigma_\theta, \sigma_\alpha, \tau_\theta, \tau_\alpha$  in Figure 7 satisfies the following relation [7]

$$\begin{cases} \sigma_\theta = \frac{1}{2}(\sigma_1 + \sigma_3) + \frac{1}{2}(\sigma_1 - \sigma_3) \cos 2\theta \\ \sigma_\alpha = \frac{1}{2}(\sigma_1 + \sigma_3) + \frac{1}{2}(\sigma_1 - \sigma_3) \cos 2\alpha \\ \tau_\theta = \frac{1}{2}(\sigma_1 - \sigma_3) \sin 2\theta \\ \tau_\alpha = \frac{1}{2}(\sigma_1 - \sigma_3) \sin 2\alpha \end{cases}$$

Under these forces, the rock will undergo shear rupture along the direction of  $\tau_\theta$ , the condition of which is,

$$\tau_\theta = \tau_f$$

$\tau_f$  is the shear strength of the rock at the corresponding temperature, and the shear strength satisfies that

$$\tau_f = \sigma_\theta \tan \theta_c + c$$

The  $\theta_c$  is the internal friction angle of the rock, which is related to the properties of the rock itself and the temperature. The  $c$  is the cohesion of the rock, also related to the two factors.

## 2.2 Mechanical properties of basalt

### 2.2.1 The tensile strength of basalt

The tensile strength  $\sigma_{max}$  of basalt is about 18.5MPa. According to the previous analysis, it is established that

$$\sigma_1 \approx \sigma_{max} = 18.5MPa$$

### 2.2.2 The shear strength of basalt

Because of lack of relevant experimental data of basalt at a high temperature, this paper uses the data of feldspar sandstone for simple estimation.

The reason why to choose feldspar sandstone is the quartz content in the feldspar sandstone is small, the basalt contains hardly quartz, and the degree of resemblance between the two rocks is high (the quartz will melt around 600°C, so it has a great influence on the cohesion of the rock and the size of the internal friction angle) [9].

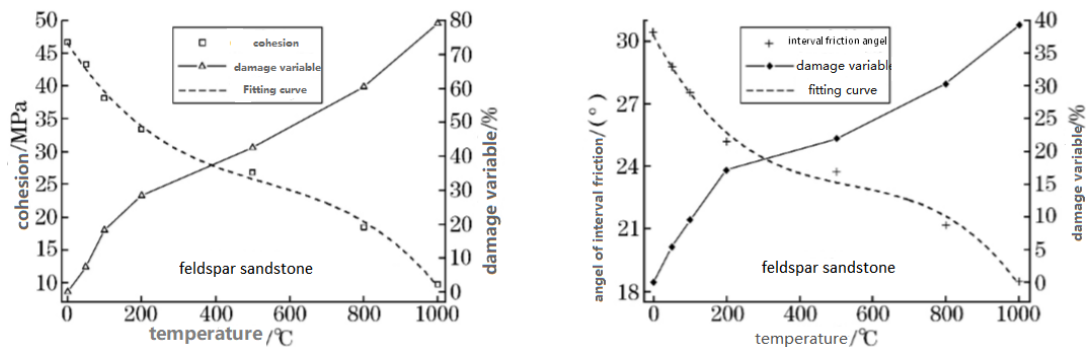


Figure 8: Relationship between cohesion/angle of internal friction and temperature of feldspar sandstone

Approximately, the relationship between internal friction angle  $\theta_c$  of feldspar sandstone and temperature is [9]

$$\theta_c = 30.27 - 0.03T + 5.35 \times 10^{-5}T^2 - 3.28 \times 10^{-8}T^3$$

The relationship between cohesion  $c$  of feldspar sandstone and temperature approximately satisfies that

$$c = 46.53 - 0.09 \times T + 1.28 \times 10^{-4}T^2 - 8.02 \times 10^{-8}T^3$$

The basalt and feldspar sandstone are brittle at 200°C, and both melt at 1000°C. Their properties are similar. Since there is almost no quartz in basalt, in order to eliminate the influence of quartz, this article takes the connection between 200°C and 1000°C of feldspar sandstone as the relationship curve between interval friction angle/cohesion of basalt and temperature, simply estimating the properties of basalt by the two points (200,33.01) and (1000,4.33).

Approximately, the relationship between internal friction angle  $\theta_c$  of basalt and temperature is

$$\theta_c = -6.48 \times 10^{-3}T + 27.45$$

The relationship between cohesion  $c$  of basalt and temperature approximately meets that

$$c = -3.59 \times 10^{-2}T + 40.19$$

### 2.3 Numerical calculation

After elimination, it can be found that  $\theta$  satisfies the following relation

$$\frac{\sigma_1 + \sigma_3}{\sigma_1 - \sigma_3} \sin \theta_c + \frac{2c}{\sigma_1 - \sigma_3} \cos \theta_c = \sin(2\theta - \theta_c)$$

According to the mechanical properties of basalt, the results of the numerical calculation are as follows,

| T    | $\theta_c$ | c     | v    | $\sigma_1$ (MPa) | $\sigma_3$ (MPa) | $\sin(2\theta - \theta_c)$ | $\theta$ |
|------|------------|-------|------|------------------|------------------|----------------------------|----------|
| 600  | 23.562     | 18.65 |      |                  |                  | 2.298362                   | #NUM!    |
| 700  | 22.914     | 15.06 |      |                  |                  | 1.465965                   | #NUM!    |
| 800  | 22.266     | 11.47 | 0.28 | 18.5             | 25.69444         | 0.624601                   | 30.46925 |
| 900  | 21.618     | 7.88  |      |                  |                  | -0.22539                   | 4.292835 |
| 1000 | 20.97      | 4.29  |      |                  |                  | -1.08366                   | #NUM!    |

Figure 9: Results of the numerical calculation

Given that the rock will undergo shear rupture along the direction of  $\tau_\theta$  in Figure 6 under these forces, there is no harming in Considering  $\theta$  in Figure 6 as the half of the centre angle of hexagonal like the following picture, and then it is intuitive that basalt tends to hexagonal structure when undergoing shear rupture.

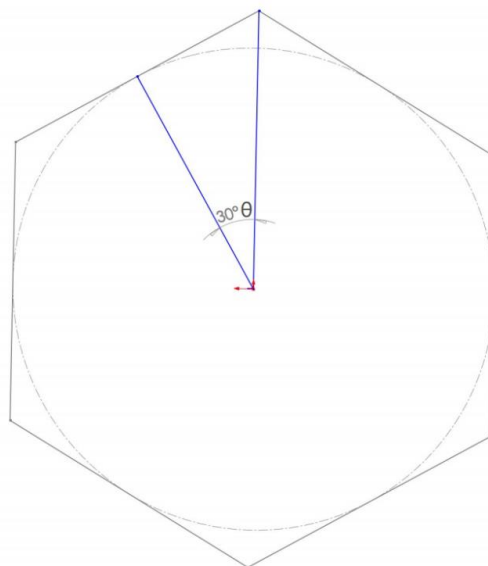


Figure 10: The schematic diagram of hexagonal, half of whose centre angle is  $\theta$

### 3. Postscript

#### 3.1 Comparison of the formation of other effusive rock columnar joints

It can be widely observed in nature that columnar joints are mainly developed in basalt, and a small amount can be seen in andesite and rhyolite. The reasons why columnar joints do not develop in such rocks are briefly analyzed as follows:

1) The cohesion of a rock. The rhyolite has a large cohesion. For one thing it appears massive after ejection from volcano, unable to form magmatic flows; For another thing, the tensile strength is large, and the tensile and shear stress are difficult to reach its shear strength in the actual cooling process.

2) The quartz content of the rock. A phase transition occurs in quartz at 600°C, which makes the volume of rock and the fluidity suddenly increase, thus changing the cooling process of rock.

#### 3.2 Analysis of formation mechanism of other columns

Besides the hexagonal prism, there are also triangular prisms, quadrangular prisms, pentagonal prisms and heptagon prisms in nature, but their distribution is different (Figure 11) [10]

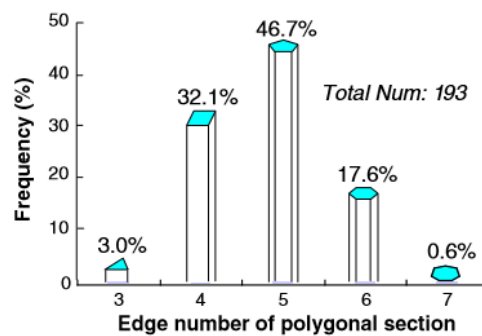


Figure 11: Statistical chart of columnar joints at the junction of Sichuan and Yunnan

The composition of magma in different regions is different, and the cohesion of rock is affected by its quartz content. As the cohesion of the rock increases, the angle between the direction of rupture and the  $\sigma_1$  becomes smaller. The rock tends to form pentagonal prism, quadrangular prism or triangular prism, and, conversely, it tends to form heptagon prism. The temperature of magma ejection and the difference of cooling rate caused by environment both affect the angle  $\theta$  of rock rupture, resulting in different shapes of columnar joints [9].

The above analysis can be further quantitatively confirmed in subsequent studies.

### 4. Conclusion

Through the analysis of the stress basalt bears during cooling, it is proposed that when the cohesion of condensation-contraction of rock (magma) reaches its tensile strength, the stress state at the micro potential fracture surface is reformed due to the Poisson effect of rock, and a new potential fracture surface is formed. When the shear stress at the new potential fracture surface is equal to the tensile strength of the rock, shear rupture occurs in the rock (magma) like the theoretical model. According to the internal friction angle, cohesion, tensile strength and Poisson's ratio of basalt at the corresponding temperature, the inner angle of columnar joint is 119.1°, which reasonably explains the formation of hexagonal shape. At last, the influence of cohesion on the shape and formation of columnar joints is discussed by comparing different rocks.

### References

[1] J. C. Phillips, M. C. S. Humphreys, K. A. Daniels, R. J. Brown, F. Witham. The formation of columnar joints produced by cooling in basalt at Staffa, Scotland. *Bulletin of Volcanology*, 2013, Vol.75 (6), pp.1-17.



- [2] Quanhai Li, Huan Zhang. *A preliminary study on the characteristics and genesis of columnar joint group in Hua'ao Island, Xiangshan County [J]. Resources, Environment and Engineering*, 2013, 27(05): 640-642 655.
- [3] Shiming Fang, Jiangfeng Li, Shiliang Wu, Guo Xu. *Geogenetic significance of hexagonal columnar joint structure of large-scale acidic volcanic rocks in Hong Kong, China [J]. Marine Science*, 2011, 35(05): 89-94.
- [4] Hailong Zhang, Chenglu Hao, Hongju Hao. *Characteristics of columnar joints and comprehensive evaluation of volcanic rocks in Xiangzhide, Duran, Qinghai Province [J]. China Metal Bulletin*, 2018(08): 284-286.
- [5] Jianli Sui. *The genetic mechanism of basalt columnar joints—local Bernard convection model [C]. China mineral rock geochemistry society. Abstract of the 15th Annual Conference of the Chinese Society of Mineral Rock Geochemistry (1). China Mineral Rock Geochemistry Society: China Mineral Rock Geochemistry Society*, 2015: 159.
- [6] Chunsheng Zhang, Yongsheng Zhu, Weijiang Chu, Ning Liu. *Mechanical Properties and Hoek-Brown Constitutive Model of Cryptographic basalt in Baihetan Hydropower Station [J]. Journal of Rock Mechanics and Engineering*, 2019, 38(10): 1964-1978.
- [7] Yadong Zheng, Tao Wang, Mingbo Ma, Gregory. A. Davis. *Maximum effective moment criterion and the origin of low-angle normal faults [J]. Journal of Structural Geology*, 2004, 26(2).
- [8] Xiangguo Kong. *Comparative Analysis of Effective Stress and Total Stress Strength and Its Indexes[J]. Western Prospecting Works*, 2005(05): 33-34.
- [9] Xingfen Ming, Xiaodong Ming. *Experimental Study on Damage Effect of the Mechanical Properties of rock in High Temperature Environment [J]. Mining Research and Development*, 2017, 37(05): 40-43.
- [10] Quan Jiang, Xia-ting Feng, Yossef H. Hatzor, Xian-jie Hao, Shao-jun Li. *Mechanical anisotropy of columnar jointed basalts: An example from the Baihetan hydropower station, China. Engineering Geology* 175 (2014) 35-45.